

Diagnostic Certificates of Data Quality and Regression Identifiability for Koopman Identification

Yue Wu^{1,2}

¹School of Automation Science and Engineering, Xi'an Jiaotong University, Xi'an 710049,
China

²Xinjiang Cigarette Factory, Hongyun Honghe Tobacco (Group) Co., Ltd., Urumqi 830000,
China

May 12, 2026

Abstract

Classical persistent excitation criteria usually assess whether an input or regressor signal is sufficiently rich. In Koopman and EDMD with control (EDMDc), however, data quality is determined by the concatenation of lifted state features and control inputs. Input-rich data can still visit a narrow state region, well-spread state samples can still produce degenerate lifted features, and both can fail to condition the final regression problem.

This paper develops a diagnostic certificate framework for locating these failures. The certificates separate state-space coverage and clustering, lifted-feature nondegeneracy, and the final regression spectrum. The regression-spectrum certificate is the layer with direct theoretical guarantees: it controls the active standardized design's smallest singular value, has Fisher-information and one-step EDMDc stability interpretations, and admits a finite-sample lower bound under a population spectral gap. We also give structural examples and a Schur-complement condition showing why state, lifted, input, and regression diagnostics cannot be substituted for one another.

As a sampling example, IGPE-DOPT uses these certificates to score candidate trajectory segments. Experiments on Duffing, Van der Pol, and Lorenz systems compare input-, state-, lifted-, and regression-oriented baselines. The results show that certificate layers separate, budget and weights shift bottlenecks, and downstream prediction or control performance is not monotone in any single certificate. The framework is therefore intended as an interpretable diagnostic and data-collection guide, not as a universal optimality claim.

Keywords: Koopman operator; EDMDc; data quality; persistent excitation; geometric certificates; regression identifiability; optimal experimental design

1 Introduction

Nonlinear dynamical systems arise broadly in fluids, chemical processes, robotics, energy systems, and biological systems. Prediction and control of such systems require a balance between model

expressiveness and computational tractability. The Koopman operator framework introduces tools from linear systems theory into nonlinear dynamics by lifting nonlinear state evolution to a linear operator acting on observable functions. Extended dynamic mode decomposition (EDMD) and EDMD with control (EDMDc) turn this idea into finite-dimensional regression problems.

For controlled systems, EDMDc fits a linear map from the current lifted state and the control input to the next lifted state. The quality of the identified model is therefore governed by a joint regression object: the visited states, the dictionary evaluations on those states, and the applied controls all enter the same least-squares design. This point is easy to obscure if classical persistent-excitation language is imported too directly. A signal can be rich in the input channel while the realized state trajectory remains confined to a narrow region. State samples can appear well spread while the selected dictionary is nearly constant or highly correlated on that region. Lifted features can be individually nondegenerate while the final lifted-state/control regression remains ill conditioned because the control columns are redundant with the lifted-state columns.

This structure reveals a multilayer data-quality problem in Koopman identification. The first layer is state-space geometry: whether trajectories cover the target region, whether directions are sufficiently diverse, and whether samples cluster locally. The second layer is lifted-feature geometry: whether the fixed dictionary forms a nondegenerate active feature space on these state samples. The third layer is regression-space geometry: whether lifted features and control inputs, after concatenation, form a regression matrix that can be estimated stably. These layers are related, but they are not interchangeable.

The goal of this paper is not to redefine classical persistent excitation or to propose a universally optimal sampler. The goal is more specific: for data collection in Koopman/EDMDc with a fixed dictionary, we provide computable and ablable diagnostic certificates that separate where data quality is gained or lost. The paper emphasizes two principles. First, the spectral condition of the final active standardized regression matrix should be inspected directly, because that is the layer closest to estimation stability. Second, upstream geometric certificates should still be reported, because they explain why the final regression object becomes ill conditioned and which layer should be repaired by subsequent data collection.

The empirical part is therefore organized as a diagnostic evidence chain rather than as a winner-takes-all benchmark. We compare IGPE-DOPT with classical input-probing and design baselines, including adaptive PE-style probing (A-PE), deterministic multisine/chirp optimal-input probing (OID), state-geometric GPE collection, random and Sobol sampling, state-space k-center selection, lifted D-optimal design, regression D-optimal design, and regression E-optimal design. These baselines test whether the proposed certificates explain the differences among input-rich, state-covering, lifted-space, and regression-space acquisition rules.

The contributions are as follows.

1. **Multilayer diagnostic certificates.** We define directional coverage, Frostman-type non-clustering, state isotropy, lifted-feature isotropy, regression isotropy, and a bottleneck-style composite certificate. We specify their standardization, active-column handling, and interpretation boundaries.
2. **Regression-identifiability theory.** We prove that the final regression-spectrum certificate is directly connected to the minimum singular value of the active standardized design, a Fisher-type information quantity, and one-step EDMDc estimation stability under a fixed design matrix. We also give a population-to-sample lower bound for the regression spectrum.
3. **Non-interchangeability of layers.** We use counterexamples to show that state geometry does not imply lifted or regression geometry, and we use a Schur-complement condition to show that

nondegenerate lifted features or input variance alone is insufficient to guarantee nondegeneracy of the full regression matrix.

4. **Certificate-driven sampling and an evidence-chain experiment.** We use IGPE-DOPT to show how certificates enter data acquisition. Using the real project evidence in Tables 2–5 and Figures 3–5, we demonstrate certificate-layer separation, regression-theory correspondence, budget and weight sensitivity, and nonmonotonicity in downstream tasks.

The rest of the paper is organized as follows. Section 2 reviews persistent excitation, data informativity, space-filling design, and Koopman data acquisition. Section 3 gives the standardized EDMDC formulation. Section 4 defines the diagnostic certificates. Section 5 gives theoretical guarantees and boundaries. Section 6 introduces IGPE-DOPT and the comparison methods. Section 7 reports experiments. Section 8 discusses limitations. Section 9 concludes.

2 Related Work

2.1 Persistent excitation and data informativity

Classical PE theory shows that, in adaptive control and linear system identification, parameter directions can be sufficiently excited if the input or regressor signal satisfies excitation conditions of sufficient order [Narendra and Annaswamy, 1987, Willems et al., 2005]. The data-informativity framework further emphasizes that whether data are sufficient depends on the target task: stabilization, prediction, and full model identification require different information [van Waarde et al., 2020]. This paper adopts this task-related viewpoint, but specializes the task object to the active standardized regression matrix of EDMDC.

2.2 Information matrices and optimal experimental design

Optimal experimental design has long used Fisher information matrices, D-optimality, and E-optimality to characterize parameter-estimation quality [Hjalmarsson, 2005, Deflorian and Zaglauer, 2011, De Cock et al., 2016, Wilson et al., 2014]. These methods are, at their core, spectral-geometric methods for regression matrices. The certificate C_{reg} is consistent with this tradition, but it is embedded in the lifted-feature/input concatenation structure of EDMDC. The distinction in this paper is the explicit separation of state, lifted-feature, and regression diagnostic layers, rather than reducing all diagnostics to a single information-matrix score.

The experimental baselines reflect this lineage. The OID baseline uses deterministic multi-sine/chirp probing as a practical optimal-input-design surrogate. The REG-DOPT and REG-EOPT baselines isolate log-determinant and minimum-eigenvalue objectives in the final regression space, while LIFT-DOPT applies the same design logic before input concatenation. These are not treated as straw-man baselines: they represent plausible ways a practitioner might collect data if the only objective were input richness, lifted-feature diversity, or regression information.

2.3 Space-filling design and state coverage

Space-filling input design for nonlinear system identification shows that a rich input spectrum is insufficient to guarantee nonlinear model quality; coverage of the state space or of the joint input-state space is also important [Kiss et al., 2024, Liu et al., 2025, Smits and Nelles, 2024]. We incorporate this viewpoint but emphasize that state coverage is only an upstream diagnostic. For EDMDC, dictionary lifting and concatenated regression can reintroduce degeneracy, so lifted-feature geometry and regression geometry must still be inspected.

2.4 Koopman/EDMDc identification and data acquisition

The Koopman/EDMD literature has studied active learning, generalized PE, fundamental-lemma-type results with Koopman embeddings, regularization, and sampling distributions [Williams et al., 2015, Proctor et al., 2016, Korda and Mezić, 2018, Brunton et al., 2022, Abraham and Murphey, 2019, Boddupalli et al., 2019, Shang et al., 2024, Dahdah and Forbes, 2022, Philipp et al., 2025]. These works provide different views of data requirements in Koopman identification. This paper focuses on reportable diagnostics for a finite dataset: given the data, dictionary, and inputs, how can one determine whether the data-quality bottleneck lies in the state space, lifted space, or final regression space?

Our GPE-STATE baseline is closest in spirit to geometry-aware active exploration: it uses state-space certificate improvement as the main acquisition signal. In contrast, IGPE-DOPT mixes state, lifted, and regression objectives. This distinction is important for positioning the algorithmic contribution. IGPE-DOPT is not presented as a universal active-learning replacement for prior Koopman acquisition methods. It is an instantiation showing how the proposed diagnostics can be turned into a data-collection rule and compared against input-, state-, lifted-, and regression-oriented alternatives.

2.5 Coverage exploration, finite excitation, and control tasks

Results on ergodic exploration, coverage control, finite excitation, and fast stabilization in reinforcement learning all show that data quality can be characterized through coverage, information-matrix spectra, or minimum eigenvalues of regression matrices [Miller et al., 2016, Rickenbach et al., 2024, Parikh et al., 2019, Lale et al., 2022]. We apply these ideas to hierarchical diagnostics for Koopman/EDMDc, but we do not compress all certificates into a new PE condition.

3 Problem Formulation and Standardized EDMDc Framework

Consider a discrete-time controlled system

$$x_{k+1} = f(x_k, u_k), \quad x_k \in \mathbb{R}^{n_x}, \quad u_k \in \mathbb{R}^{n_u}. \quad (1)$$

The dataset is

$$\mathcal{D}_N = \{(x_k, u_k, x_{k+1})\}_{k=1}^N. \quad (2)$$

For a dictionary $\psi : \mathbb{R}^{n_x} \rightarrow \mathbb{R}^{d_\psi}$, define the augmented regressor

$$\xi_k = \begin{bmatrix} \psi(x_k) \\ u_k \end{bmatrix} \in \mathbb{R}^p, \quad p = d_\psi + n_u. \quad (3)$$

Stacking samples gives

$$\Phi = \begin{bmatrix} \xi_1^\top \\ \dots \\ \xi_N^\top \end{bmatrix}, \quad Y = \begin{bmatrix} \psi(x_2)^\top \\ \dots \\ \psi(x_{N+1})^\top \end{bmatrix}. \quad (4)$$

EDMDc solves

$$\min_K \|Y - \Phi K\|_F^2. \quad (5)$$

The geometry of this problem is determined by $\Phi^\top \Phi$. If $\Phi^\top \Phi$ has small eigenvalues, some lifted/input directions have not been sufficiently excited by the data, and the least-squares estimate is sensitive to noise. Classical input PE inspects only the input sequence and does not directly guarantee the spectral condition of this concatenated matrix.

3.1 Active standardized coordinates

The columns of the raw regression matrix Φ may have very different scales. For example, polynomial features can be much larger than input columns, and a constant observable produces a zero-variance column. This paper defines spectral certificates in centered and active-column standardized coordinates. Write

$$\Phi = \mathbf{1}\mu_\Phi^\top + \bar{\Phi}D_\Phi, \quad (6)$$

where μ_Φ is the column mean, D_Φ is the active-column scale matrix, and $\bar{\Phi}$ is the active standardized regression matrix. If a column variance is below a numerical threshold, that column is not included in the active spectral certificate, but the active dimension or active rank must be reported explicitly.

The standardized regression is written as

$$\bar{Y} = \bar{\Phi}\bar{K} + E. \quad (7)$$

All theoretical results act on these active standardized coordinates. If the full unscreened dictionary contains zero-variance directions, then the minimum eigenvalue of the full Gram matrix is naturally zero. We do not silently hide this degeneracy with regularization; instead, we require reporting active dimensions, active ranks, and spectral quantities.

4 Data-Quality Diagnostic Certificates

The certificates are defined in the order in which data enter the EDMDC regression. State-space certificates are indirect diagnostics. Lifted- and regression-space certificates are closer to the final estimation problem. Regression isotropy C_{reg} is the directly provable certificate.

4.1 State-space certificates

Directional coverage. Let

$$d_k = \frac{x_{k+1} - x_k}{\|x_{k+1} - x_k\|_2 + \epsilon} \quad (8)$$

be a unit displacement direction in the whitened state space. For a set of angular resolutions $\Delta = \{\delta_\ell\}$, let M_ℓ be the maximum greedy count of a δ_ℓ -separated direction set, and let M_ℓ^* be the reference target count. Define

$$C_{\text{dir}} = \min_\ell \frac{M_\ell}{M_\ell^*}. \quad (9)$$

A larger value indicates more dispersed trajectory directions. This certificate alone does not imply a regression error bound.

Frostman-type non-clustering. Let \tilde{x}_i denote a whitened state sample and let s be a reference dimension. For a set of scales \mathcal{R} , define

$$\rho(r) = \max_i \frac{\frac{1}{N} \sum_{j=1}^N \mathbf{1}\{\|\tilde{x}_j - \tilde{x}_i\|_2 \leq r\}}{r^s + \epsilon}. \quad (10)$$

The non-clustering certificate is

$$C_{\text{fr}} = \min_{r \in \mathcal{R}} \frac{\rho_{\max}}{\rho(r)}. \quad (11)$$

This certificate diagnoses local repeated sampling and multiscale clustering. It is an empirical diagnostic and is not equivalent to a strict Frostman measure condition.

State isotropy. For the active standardized matrix \bar{X} of the state sample matrix X , define

$$C_{\text{state}} = \lambda_{\min} \left(\frac{1}{N} \bar{X}^\top \bar{X} \right). \quad (12)$$

In the experiments, `state_iso` is this quantity normalized by a fixed display threshold.

4.2 Lifted- and regression-space certificates

Lifted-feature isotropy. For the active standardized matrix $\bar{\Psi}$ of the lifted-feature matrix $\Psi = [\psi(x_1)^\top; \dots; \psi(x_N)^\top]$, define

$$C_{\text{lift}} = \lambda_{\min} \left(\frac{1}{N} \bar{\Psi}^\top \bar{\Psi} \right). \quad (13)$$

This certificate detects whether the dictionary produces nearly constant columns, zero columns, or highly correlated directions under the sampled distribution.

Regression isotropy. For the active standardized matrix $\bar{\Phi}$ of the concatenated regression matrix $\Phi = [\Psi, U]$, define

$$C_{\text{reg}}(\mathcal{D}_N) = \lambda_{\min} \left(\frac{1}{N} \bar{\Phi}^\top \bar{\Phi} \right). \quad (14)$$

This certificate acts directly on the final EDMDC least-squares problem. It is not a simple function of `state_iso`, `lift_iso`, or input variance, because the concatenated matrix can degenerate due to correlations between lifted-feature columns and input columns.

Bottleneck-style composite certificate. To report an overall data-quality profile, we use

$$C_{\text{GPE}} = \min\{C_{\text{dir}}, C_{\text{fr}}, C_{\text{rad}}, C_{\text{state}}/\tau_{\text{state}}, C_{\text{lift}}/\tau_{\text{lift}}, C_{\text{reg}}/\tau_{\text{reg}}\}. \quad (15)$$

Here $\tau_{\text{state}} = 0.20$, $\tau_{\text{lift}} = 0.05$, and $\tau_{\text{reg}} = 0.05$ are experimental display thresholds, not theoretical constants. The composite certificate is used to localize bottlenecks and is not a performance guarantee.

5 Theoretical Guarantees and Boundaries

5.1 Finite-sample regression stability

Consider the standardized EDMDC regression under a fixed design matrix. For a general finite dictionary, we do not assume that the true system is exactly represented by the dictionary. Define the empirical projection target

$$K_N^* = \arg \min_K \|\bar{Y} - \bar{\Phi}K\|_F^2, \quad (16)$$

and write

$$\bar{Y} = \bar{\Phi}K_N^* + R_N + E, \quad \bar{\Phi}^\top R_N = 0. \quad (17)$$

If $C_{\text{reg}}(\mathcal{D}_N) > 0$, then

$$\sigma_{\min}(\bar{\Phi}) = \sqrt{NC_{\text{reg}}(\mathcal{D}_N)}. \quad (18)$$

If the noise rows satisfy a conditional Gaussian model $e_k \sim \mathcal{N}(0, \Sigma_e)$ and are mutually independent, then the Fisher-type information matrix is

$$\mathcal{I}_N = \Sigma_e^{-1} \otimes (\bar{\Phi}^\top \bar{\Phi}), \quad (19)$$

and satisfies

$$\lambda_{\min}(\mathcal{I}_N) \geq \frac{NC_{\text{reg}}(\mathcal{D}_N)}{\lambda_{\max}(\Sigma_e)}. \quad (20)$$

The ridge estimate

$$\widehat{K}_\lambda = (\bar{\Phi}^\top \bar{\Phi} + \lambda I)^{-1} \bar{\Phi}^\top \bar{Y} \quad (21)$$

satisfies

$$\|\widehat{K}_\lambda - K_N^*\|_F \leq \frac{\|\bar{\Phi}^\top E\|_F + \lambda \|K_N^*\|_F}{NC_{\text{reg}}(\mathcal{D}_N) + \lambda}. \quad (22)$$

If the noise rows are conditionally independent, zero-mean, and have covariance bounded by $\sigma^2 I_q$, then the least-squares estimate satisfies

$$\mathbb{E} \left[\|\widehat{K}_0 - K_N^*\|_F^2 \mid \bar{\Phi} \right] \leq \frac{\sigma^2 qp}{NC_{\text{reg}}(\mathcal{D}_N)}. \quad (23)$$

This result controls only one-step EDMDC regression stability in active standardized coordinates. It does not control finite-dictionary approximation error, Koopman invariant-subspace error, long-horizon rollout error propagation, or closed-loop control performance.

5.2 From sampling distributions to empirical regression spectra

Let $\xi \in \mathbb{R}^p$ be an active regressor sampled from a distribution ρ . The theoretical standardization uses population means and scales:

$$\bar{\xi}_\rho = D_\rho^{-1}(\xi - \mu_\rho), \quad \mu_\rho = \mathbb{E}_\rho[\xi]. \quad (24)$$

Define

$$G_\rho = \mathbb{E}_\rho[\bar{\xi}_\rho \bar{\xi}_\rho^\top]. \quad (25)$$

If $\lambda_{\min}(G_\rho) \geq \mu > 0$ and independent samples satisfy

$$\left\| \frac{1}{N} \sum_{k=1}^N \bar{\xi}_{\rho,k} \bar{\xi}_{\rho,k}^\top - G_\rho \right\|_2 \leq \frac{\mu}{2}, \quad (26)$$

then

$$C_{\text{reg}}^\rho(\mathcal{D}_N) \geq \frac{\mu}{2}. \quad (27)$$

If, additionally, $\|\bar{\xi}_{\rho,k}\|_2 \leq R$, a matrix Bernstein-type inequality gives that

$$N \gtrsim \frac{R^2}{\mu} \log \frac{p}{\delta} \quad (28)$$

is sufficient to control the above deviation event with high probability. The sample-standardized `regression_iso` used in the experiments is a finite-sample computable substitute for this theoretical object.

5.3 Identifiability bridge and Schur-complement condition

Suppose the state distribution has a density lower bound on a compact set Ω , and the active dictionary ψ_A is continuous and linearly independent modulo constants in $L_2(\Omega)$. Then the population Gram matrix of the centered lifted features satisfies

$$A_\rho \succeq \alpha I, \quad \alpha > 0. \quad (29)$$

If the residual of the input relative to the linear projection onto the lifted features satisfies

$$S_{U|\Psi,\rho} = \mathbb{E}[(u - \Pi_{\psi_A} u)(u - \Pi_{\psi_A} u)^\top] \succeq \beta I, \quad (30)$$

then the population Gram matrix of the full regressor satisfies

$$\lambda_{\min}(G_\rho) \geq \frac{\min\{\alpha, \beta\}}{(1 + \gamma_\rho)^2}. \quad (31)$$

This statement shows that a positive regression spectral lower bound requires three classes of conditions to work together: the state distribution must cover the target region, the dictionary must be nondegenerate on that region, and the input must have conditional excitation relative to the lifted features.

5.4 Counterexample for layer separation

Consider the two-dimensional sample set

$$\mathcal{X} = \{(1, 0), (-1, 0), (0, 1), (0, -1)\}. \quad (32)$$

Its state covariance is $\Sigma_x = \frac{1}{2}I_2$, so the state geometry is favorable. If the quadratic dictionary

$$\psi(x) = [x_1, x_2, x_1^2, x_1x_2, x_2^2]^\top \quad (33)$$

is used, then $x_1x_2 = 0$ for every sample. The column corresponding to x_1x_2 in the lifted matrix is identically zero, and both the lifted Gram matrix and the full regression Gram matrix are singular. Thus, state geometry cannot in general imply lifted or regression geometry. This counterexample explains why `state_iso`, `lift_iso`, and `regression_iso` must all be reported.

5.5 Submodular D-optimal boundary

Given a finite candidate library \mathcal{V} of trajectory segments, suppose each candidate segment i contributes a regression block matrix Φ_i . Define the pure regression D-optimal objective

$$F(S) = \log \det \left(\epsilon I + \sum_{i \in S} \Phi_i^\top \Phi_i \right). \quad (34)$$

This function is monotone and submodular in the set S . Therefore, under a fixed candidate library and a fixed budget, the greedy algorithm that selects the largest marginal gain at each step has the classical $(1 - 1/e)$ approximation guarantee. The full IGPE-DOPT mixed objective also contains state-coverage, directional-novelty, and clustering-penalty terms, and therefore does not inherit this global guarantee.

6 Certificate-Driven Data Acquisition: IGPE-DOPT

IGPE-DOPT is a certificate-driven sampling example. At each round, the method simulates candidate trajectory segments from a finite library of constant-input segments, appends each candidate segment to the current dataset, computes state, lifted, and regression certificates, and chooses the highest-scoring segment. The algorithm is a myopic set-building procedure, not a globally optimal sampler.

The default scoring terms match the code implementation:

Table 1: Default IGPE-DOPT scoring terms.

Term	Code key	Weight	Meaning
State minimum spectrum	<code>state_min</code>	0.75	State coverage
Lifted log-det	<code>lift_logdet</code>	0.80	Lifted D-optimality
Lifted effective rank	<code>lift_eff_rank</code>	0.35	Lifted spectral dispersion
Regression minimum spectrum	<code>reg_min</code>	0.35	Regression E-optimality
Directional novelty	<code>novelty</code>	0.30	New motion directions
Input variance	<code>u_var</code>	0.10	Input diversity
Clustering penalty	<code>cluster</code>	0.25	Non-clustering

The comparison methods are split into two categories. **External/literature-motivated baselines** are methods that represent established or natural alternatives to certificate-driven sampling: **A-PE** represents adaptive PE-style input probing; **OID** uses deterministic multisine/chirp probing as an optimal-input-design surrogate; **GPE-STATE** targets state-space geometric coverage; **RANDOM** and **SOBOL** represent undirected random and low-discrepancy sampling; **STATE-KCENTER** is a state-space space-filling k -center coverage baseline whose design intent is to maximize state coverage rather than the regression spectrum; **LIFT-DOPT** isolates lifted-space log-determinant design; **REG-DOPT** isolates regression-space log-determinant design; and **REG-EOPT** is a regression-space E-optimal design baseline whose design intent is to directly improve the minimum regression spectrum.

Internal ablation variants are used only to diagnose the contribution of components inside the proposed scoring rule. These include **IGPE-NO-DOPT**, **IGPE-NO-DIR**, **IGPE-NO-CLUSTER**, and the weight variants **IGPE-WHALF**, **IGPE-UNIFORM**, **IGPE-REG-HEAVY**, and **IGPE-CLUSTER-HEAVY**. They are not presented as external published baselines; they are controlled variants of the proposed sampler. IGPE-DOPT combines the external diagnostic layers through the mixed certificate score above.

7 Empirical Validation and Diagnostic Analysis

7.1 Experimental setup and quality checks

The experimental systems are Duffing, Van der Pol, and Lorenz. The main budget ablation uses the **major-budget-ablation** configuration: methods are **RANDOM**, **SOBOL**, **STATE-KCENTER**, **REG-EOPT**, and **IGPE-DOPT**; seeds are 0 through 9; budgets are $B \in \{8, 12, 20, 40, 80\}$; the segment length is `l_seg=12`; the time step is `dt=0.01`; the prediction horizon is 200 steps; and the control horizon is 100 steps. This configuration produces 750 cases in total.

The expanded baseline comparison uses the separate **major-revision** configuration: methods are **RANDOM**, **SOBOL**, **STATE-KCENTER**, **LIFT-DOPT**, **REG-DOPT**, **REG-EOPT**, **A-PE**, **OID**, **GPE-STATE**, and **IGPE-DOPT**; seeds are 0 through 19; the budget is fixed at $B = 40$; and all other simulation settings

are the same. This comparison is used to assess how certificate diagnostics behave against input-rich, state-covering, lifted-space, and regression-space acquisition baselines.

The quality-check file [results/geometry_major_revision_budget/tables/table5_quality_checks.csv](#) shows that all certificates, spectral quantities, one-step errors, prediction metrics, and control metrics have 750 rows; nonfinite and NaN counts are all zero; and prediction failure and control failure counts are also zero.

7.2 Scientific question 1: Do certificate layers separate?

Table 2 reports representative compressed results for the three layers: state, lifted, and regression certificates, together with active rank and active dimension. The quantities `state_iso`, `lift_iso`, and `regression_iso` use different display-threshold normalizations and should not be compared as absolute magnitudes across certificate types.

For Duffing, STATE-KCENTER has high `state_iso`, but its `regression_iso` is lower than those of REG-EOPT and IGPE-DOPT. For Van der Pol, IGPE-DOPT improves both state and regression certificates. For Lorenz, STATE-KCENTER is more favorable for lifted/regression certificates. This shows that the layer relationship is not a monotone chain, but a data-quality profile jointly determined by the system, dictionary, and sampling strategy.

7.3 Scientific question 2: Does the regression certificate correspond to theoretical quantities?

Table 3 reports the regression certificate, condition number, one-step lift/state RMSE, and active rank. The table does not treat the definitional identity between C_{reg} and $\sigma_{\min}(\bar{\Phi})$ as independent empirical evidence; that sanity check is placed in Figure 5.

The expanded comparison confirms that the baseline choice changes the diagnostic profile. REG-EOPT and GPE-STATE are favorable on Duffing regression certificates, STATE-KCENTER and LIFT-DOPT are favorable on Lorenz, and IGPE-DOPT has the largest standardized GPE index on Van der Pol. OID gives very small one-step lifted errors on Duffing and Van der Pol, but this does not imply the largest regression certificate. IGPE-DOPT obtains the lowest Lorenz tracking error in this comparison, while it is not best on Duffing or Van der Pol open-loop RMSE. These results are consistent with the theoretical boundary: `regression_iso` is the spectral bottleneck for one-step regression stability, but task metrics also depend on dictionary bias, operating region, learned operator spectrum, and closed-loop controllability.

7.4 Scientific question 3: How do budget and sampling distribution affect spectral bottlenecks?

The budget ablation covers $B \in \{8, 12, 20, 40, 80\}$ and 750 cases. Figure 3 shows that increasing the budget generally improves geometric/regression certificates, but different methods follow different paths. REG-EOPT directly targets the minimum regression spectrum. STATE-KCENTER changes the state distribution. IGPE-DOPT attempts to balance state-, lifted-, and regression-space certificates. This is consistent with the population-to-sample theory: the finite-sample spectral bottleneck is affected both by sample size and by the spectral gap of the population Gram matrix induced by the sampling distribution.

Table 2: Certificate-layer separation, reported as mean [95% CI]. The complete table is available at results/geometry_major_revision_budget/tables/table6_v4_certificate_hierarchy.md.

system	method	n	state_iso	lift_iso	regression_iso	active_rank	active_dim
duffing	RANDOM	50	2.96 [2.55, 3.35]	0.0829 [0.0373, 0.137]	0.0815 [0.0363, 0.135]	10 [10, 10]	10 [10, 10]
duffing	SOBOL	50	3.17 [2.79, 3.5]	0.0172 [0.00428, 0.0367]	0.0171 [0.00422, 0.0365]	9.98 [9.94, 10]	10 [10, 10]
duffing	STATE-KCENTER	50	4.18 [3.9, 4.41]	0.0154 [0.00539, 0.0277]	0.0126 [0.00412, 0.0235]	10 [10, 10]	10 [10, 10]
duffing	REG-EOPT	50	3.27 [2.89, 3.62]	0.132 [0.0624, 0.21]	0.131 [0.0613, 0.209]	10 [10, 10]	10 [10, 10]
duffing	IGPE-DOPT	50	4.16 [3.87, 4.43]	0.073 [0.024, 0.135]	0.0711 [0.0235, 0.132]	10 [10, 10]	10 [10, 10]
lorenz	RANDOM	50	0.549 [0.521, 0.582]	0.00572 [0.00487, 0.00679]	0.00546 [0.00456, 0.00657]	10 [10, 10]	10 [10, 10]
lorenz	SOBOL	50	0.569 [0.545, 0.597]	0.00584 [0.00489, 0.00682]	0.00561 [0.00466, 0.00659]	10 [10, 10]	10 [10, 10]
lorenz	STATE-KCENTER	50	0.598 [0.579, 0.616]	0.0114 [0.00938, 0.0136]	0.0108 [0.00864, 0.0129]	10 [10, 10]	10 [10, 10]
lorenz	REG-EOPT	50	0.611 [0.58, 0.646]	0.00551 [0.005, 0.00608]	0.00543 [0.0049, 0.00599]	10 [10, 10]	10 [10, 10]
lorenz	IGPE-DOPT	50	0.616 [0.573, 0.652]	0.0086 [0.00671, 0.0106]	0.00845 [0.00655, 0.0104]	10 [10, 10]	10 [10, 10]
vdp	RANDOM	50	2.93 [2.47, 3.37]	0.0635 [0.0339, 0.0977]	0.0628 [0.0334, 0.0967]	10 [10, 10]	10 [10, 10]
vdp	SOBOL	50	2.79 [2.3, 3.29]	0.0722 [0.042, 0.103]	0.0715 [0.0416, 0.103]	10 [10, 10]	10 [10, 10]
vdp	STATE-KCENTER	50	3.26 [2.81, 3.67]	0.0695 [0.0424, 0.0997]	0.0685 [0.0415, 0.0985]	9.96 [9.9, 10]	10 [10, 10]
vdp	REG-EOPT	50	2.96 [2.51, 3.41]	0.0881 [0.0441, 0.13]	0.0869 [0.043, 0.129]	9.8 [9.64, 9.92]	10 [10, 10]
vdp	IGPE-DOPT	50	3.97 [3.66, 4.24]	0.128 [0.0564, 0.206]	0.125 [0.0546, 0.204]	10 [10, 10]	10 [10, 10]

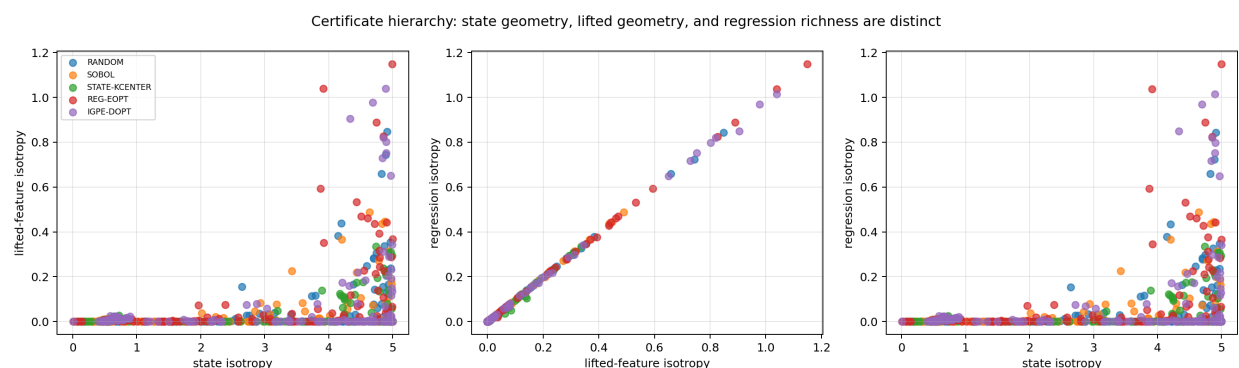


Figure 1: Certificate hierarchy and layer separation.

Table 3: Expanded baseline comparison at budget $B = 40$, reported as mean [95% CI] over 20 seeds. The underlying summary is available at results/geometry_major_revision_baselines/tables/table1_summary.csv; the regression-diagnostics table for the design baselines is available at results/geometry_major_revision_baselines/tables/table7_v4_external_baselines.md.

system	method	n	std_GPE	regression_iso	one_step_lift	open_loop	tracking
duffing	RANDOM	20	0.0565 [0.0299, 0.0888]	0.0568 [0.0299, 0.0891]	0.021 [0.0177, 0.0245]	0.000504 [0.000203, 0.000883]	0.181 [0.167, 0.193]
duffing	SOBOL	20	0.0419 [0.0165, 0.0724]	0.0419 [0.0165, 0.0724]	0.0345 [0.0263, 0.0434]	0.0011 [0.000157, 0.0025]	0.181 [0.167, 0.193]
duffing	STATE-KCENTER	20	0.0066 [0.0034, 0.0111]	0.0066 [0.0034, 0.0111]	0.0142 [0.0131, 0.0154]	0.001 [0.000509, 0.0016]	0.181 [0.167, 0.193]
duffing	LIFT-DOPT	20	0.052 [0.0213, 0.0876]	0.0628 [0.0234, 0.111]	0.0537 [0.0386, 0.0692]	0.0025 [0.000866, 0.0044]	0.181 [0.167, 0.193]
duffing	REG-DOPT	20	0.0775 [0.0422, 0.115]	0.0847 [0.0455, 0.125]	0.0453 [0.035, 0.0568]	0.000504 [0.000238, 0.000813]	0.181 [0.167, 0.193]
duffing	REG-EOPT	20	0.112 [0.0655, 0.156]	0.127 [0.0696, 0.183]	0.0242 [0.0177, 0.032]	0.000965 [0.000321, 0.002]	0.181 [0.167, 0.193]
duffing	A-PE	20	0.026 [0.0101, 0.0489]	0.0301 [0.0101, 0.0605]	0.021 [0.0177, 0.0252]	0.001 [0.000118, 0.0022]	0.181 [0.167, 0.193]
duffing	OID	20	0.0439 [0.027, 0.0608]	0.0439 [0.027, 0.0608]	0.0035 [0.0027, 0.0045]	0.000329 [0.00021, 0.000474]	0.181 [0.167, 0.193]
duffing	GPE-STATE	20	0.0934 [0.0527, 0.142]	0.112 [0.0596, 0.177]	0.013 [0.0113, 0.0146]	0.000459 [0.000159, 0.000856]	0.181 [0.167, 0.193]
duffing	IGPE-DOPT	20	0.0757 [0.0354, 0.121]	0.0819 [0.0384, 0.129]	0.053 [0.0395, 0.0686]	0.309 [0.000752, 0.923]	0.181 [0.167, 0.194]
lorenz	RANDOM	20	0.0053 [0.0045, 0.0061]	0.0053 [0.0045, 0.0061]	0.0176 [0.0169, 0.0183]	12.2 [9.8, 14.3]	2.54 [0.642, 4.71]
lorenz	SOBOL	20	0.0067 [0.0054, 0.0081]	0.0067 [0.0054, 0.0081]	0.0173 [0.0168, 0.0179]	9.3 [7, 11.6]	3.58 [1.42, 6.06]
lorenz	STATE-KCENTER	20	0.0205 [0.0197, 0.0215]	0.0205 [0.0197, 0.0215]	0.0368 [0.0358, 0.038]	7.52 [6.2, 9.23]	8.5 [5.07, 11.8]
lorenz	LIFT-DOPT	20	0.0171 [0.0151, 0.0189]	0.0171 [0.0151, 0.0189]	0.0299 [0.0275, 0.0322]	6.29 [4.85, 7.93]	2.81 [0.818, 5.54]
lorenz	REG-DOPT	20	0.0053 [0.0047, 0.006]	0.0053 [0.0047, 0.006]	0.018 [0.0176, 0.0184]	10.5 [7.98, 13]	4.77 [2.5, 7.37]
lorenz	REG-EOPT	20	0.0069 [0.0059, 0.0079]	0.0069 [0.0059, 0.0079]	0.0191 [0.0182, 0.02]	11.9 [9.54, 14.1]	3.18 [1.21, 5.47]
lorenz	A-PE	20	0.0064 [0.0055, 0.0075]	0.0064 [0.0055, 0.0075]	0.0181 [0.0174, 0.0189]	10.4 [8.12, 12.6]	3.67 [1.57, 5.99]
lorenz	OID	20	0.0044 [0.0041, 0.0049]	0.0044 [0.0041, 0.0049]	0.0169 [0.0162, 0.0176]	12.5 [10.4, 14.5]	1.45 [0.184, 3.3]
lorenz	GPE-STATE	20	0.0068 [0.0059, 0.0079]	0.0068 [0.0059, 0.0079]	0.0184 [0.0177, 0.0192]	12.1 [9.64, 14.2]	9.15 [6.23, 12]
lorenz	IGPE-DOPT	20	0.0102 [0.0085, 0.0119]	0.0102 [0.0085, 0.0119]	0.0226 [0.0209, 0.0243]	8.69 [6.81, 10.8]	0.787 [0.113, 2.13]
vdp	RANDOM	20	0.0497 [0.0374, 0.0623]	0.0497 [0.0374, 0.0623]	0.0123 [0.0103, 0.0145]	0.0529 [0.0086, 0.138]	0.181 [0.167, 0.193]
vdp	SOBOL	20	0.0711 [0.0581, 0.0853]	0.0711 [0.0581, 0.0853]	0.0139 [0.0131, 0.0148]	0.0181 [0.0098, 0.0291]	0.181 [0.167, 0.193]
vdp	STATE-KCENTER	20	0.0804 [0.0599, 0.101]	0.0804 [0.0599, 0.101]	0.0096 [0.0087, 0.0104]	0.0337 [0.0178, 0.0571]	0.18 [0.166, 0.193]
vdp	LIFT-DOPT	20	0.077 [0.0447, 0.114]	0.0791 [0.0455, 0.116]	0.0445 [0.0286, 0.062]	1.93 [0.0993, 4.77]	0.179 [0.165, 0.192]
vdp	REG-DOPT	20	0.0697 [0.0381, 0.106]	0.0721 [0.0384, 0.113]	0.0409 [0.0253, 0.0585]	0.115 [0.0189, 0.288]	0.181 [0.166, 0.193]
vdp	REG-EOPT	20	0.0819 [0.0407, 0.139]	0.115 [0.0442, 0.214]	0.0219 [0.0168, 0.0272]	0.136 [0.0319, 0.324]	0.18 [0.167, 0.192]
vdp	A-PE	20	0.0452 [0.0346, 0.0557]	0.0452 [0.0346, 0.0557]	0.0119 [0.0105, 0.0136]	0.0105 [0.0068, 0.0151]	0.181 [0.167, 0.193]
vdp	OID	20	0.0135 [0.006, 0.0244]	0.0135 [0.006, 0.0244]	0.0019 [0.0016, 0.0023]	0.0355 [0.0198, 0.056]	0.181 [0.167, 0.193]
vdp	GPE-STATE	20	0.0274 [0.012, 0.0442]	0.0274 [0.012, 0.0442]	0.0124 [0.0096, 0.0151]	0.27 [0.0321, 0.612]	0.18 [0.166, 0.192]
vdp	IGPE-DOPT	20	0.108 [0.0633, 0.158]	0.137 [0.0723, 0.237]	0.0398 [0.0277, 0.0539]	4.53 [0.054, 13.4]	0.187 [0.168, 0.212]

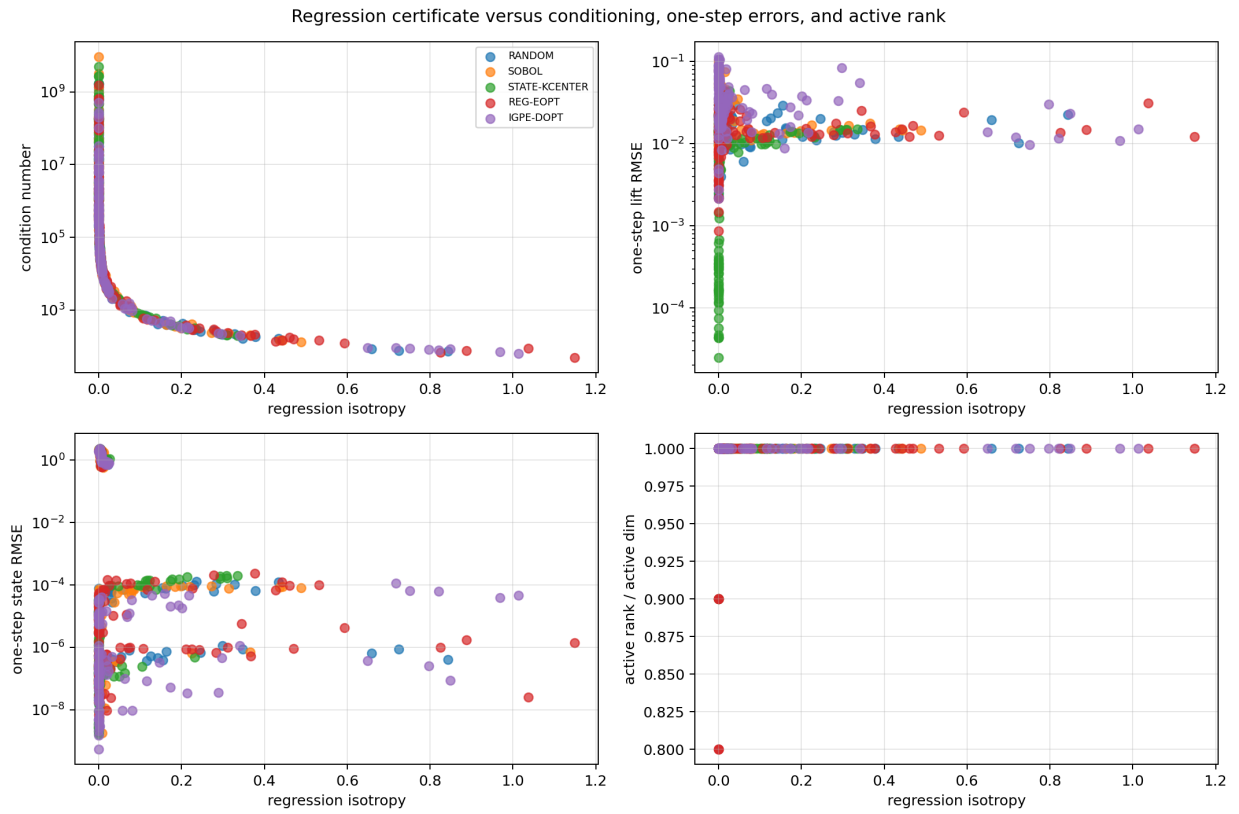


Figure 2: Regression certificate and quantities associated with the theory.

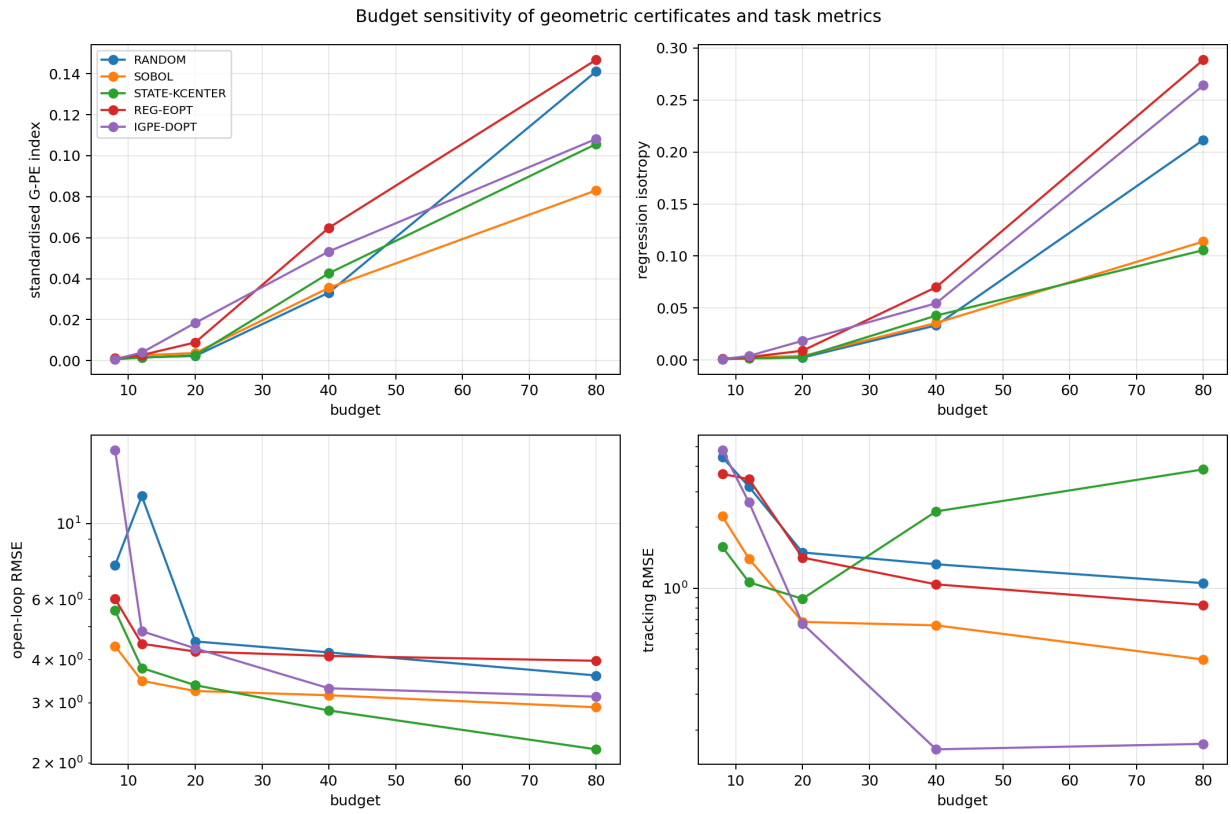


Figure 3: Budget sensitivity.

7.5 Scientific question 4: Are long-horizon prediction and closed-loop tasks monotone?

Table 4 reports open-loop RMSE, tracking RMSE, failure rates, and paired effect sizes relative to IGPE-DOPT. It shows that the regression certificate cannot be interpreted as a monotone guarantee for long-horizon prediction or closed-loop control.

On Duffing and Van der Pol, the open-loop mean of IGPE-DOPT is affected by a small number of large-error seeds. On Lorenz, the tracking RMSE of IGPE-DOPT is lower than those of RANDOM, STATE-KCENTER, and REG-EOPT, but its open-loop RMSE is not optimal. This is an empirical manifestation of the boundary of the theoretical result: one-step regression stability is not the same as long-horizon rollout stability, nor is it the same as optimality on a closed-loop task.

7.6 Scientific question 5: Weight sensitivity

Table 5 comes from the independent `weight-sensitivity` configuration: three systems, 10 seeds, budget 40, and five IGPE weight variants. The table checks whether the conclusions depend on the default manually tuned weights.

Changing weights changes the data-quality profile. In Duffing, IGPE-REG-HEAVY increases `regression_iso` to 0.149 [0.0772, 0.226]. In Lorenz, IGPE-WHALF increases `regression_iso` to 0.0142 [0.0115, 0.0165], but tracking RMSE rises to 3.03 [0.137, 7.3]. This shows that increasing one certificate does not guarantee optimality across all downstream tasks.

7.7 Computational cost

No manuscript-scale per-method timing logs were available in the existing result directories, so we ran a lightweight local benchmark on the same script path. The benchmark used Windows 10, Python 3.8.10, an Intel Core Ultra 5 125H CPU with 14 cores and 18 logical processors, and 31.5 GiB RAM. Each entry in Table 6 is the mean wall-clock time over three single-system cases (Duffing, Van der Pol, and Lorenz) with seed 0, budget $B = 8$, segment length 8, time step 0.01, prediction horizon 40, and control horizon 20. The timings call the internal case runner and exclude file export and figure generation, so they should be interpreted as empirical low-dimensional guidance for relative cost rather than as manuscript-scale runtimes.

7.8 Appendix figure for a definitional identity

Figure 5 shows the sanity check between C_{reg} and $\sigma_{\min}(\bar{\Phi})$. Because they satisfy the definitional identity $\sigma_{\min}(\bar{\Phi}) = \sqrt{NC_{\text{reg}}}$, the figure is used only as an implementation check and not as an independent empirical finding.

8 Discussion and Limitations

The claim of this paper is diagnostic. Data quality for Koopman/EDMDc should not ask only whether the input is PE; it should ask whether the population Gram matrix and finite-sample Gram matrix of the active standardized regressor have sufficient spectral gaps. State coverage, non-clustering, and directional diversity explain the sampling-distribution layer. Lifted and regression isotropy explain the dictionary layer and the final regression layer.

The paper has four main boundaries. First, we do not prove that directional coverage or Frostman non-clustering implies a lower bound on C_{reg} for general dictionaries and general dynamical systems. Second, IGPE-DOPT is a mixed heuristic sampler; the full objective has no global optimality or approximate-optimality guarantee. Third, the regression theory controls only one-step EDMDc

Table 4: Downstream prediction/control metrics, reported as mean [95% CI]. The complete table is available at `results/geometry_major_revision_budget/tables/table8_v4_downstream_tasks.md`.

system	method	open_loop_rmse	tracking_rmse	prediction_failure_rate	control_failure_rate	dz_open_loop_vs_IGPE	dz_tracking_vs_IGPE
duffing	RANDOM	0.00557 [0.00305, 0.00893]	0.181 [0.176, 0.186]	0	0	-0.128	0.196
duffing	SOBOL	0.00731 [0.00134, 0.0172]	0.181 [0.176, 0.186]	0	0	-0.0619	-0.0791
duffing	STATE-KCENTER	0.00188 [0.000984, 0.00309]	0.181 [0.176, 0.186]	0	0	-0.225	0.329
duffing	REG-EOPT	0.0037 [0.00146, 0.00644]	0.181 [0.176, 0.186]	0	0	-0.169	0.183
duffing	IGPE-DOPT	0.0106 [0.00322, 0.0232]	0.181 [0.176, 0.186]	0	0	0	0
lorenz	RANDOM	13.9 [11.6, 17.3]	6.53 [4.87, 8.33]	0	0	-0.0536	0.196
lorenz	SOBOL	9.82 [8.38, 11.3]	2.91 [1.73, 4.33]	0	0	-0.186	-0.221
lorenz	STATE-KCENTER	10.6 [8.38, 13.6]	5.53 [3.76, 7.38]	0	0	-0.157	0.0812
lorenz	REG-EOPT	12.2 [11.1, 13.3]	5.87 [3.97, 7.8]	0	0	-0.108	0.121
lorenz	IGPE-DOPT	15.6 [10.5, 25.2]	4.73 [2.99, 6.66]	0	0	0	0
vdv	RANDOM	5.26 [0.768, 13.2]	0.182 [0.176, 0.19]	0	0	0.0549	0.0898
vdv	SOBOL	0.471 [0.127, 0.939]	0.18 [0.176, 0.185]	0	0	-0.208	-0.114
vdv	STATE-KCENTER	0.0856 [0.0479, 0.138]	0.181 [0.176, 0.186]	0	0	-0.236	0.113
vdv	REG-EOPT	1.48 [0.432, 2.73]	0.208 [0.182, 0.254]	0	0	-0.134	0.184
vdv	IGPE-DOPT	3.54 [0.603, 8.53]	0.181 [0.176, 0.186]	0	0	0	0

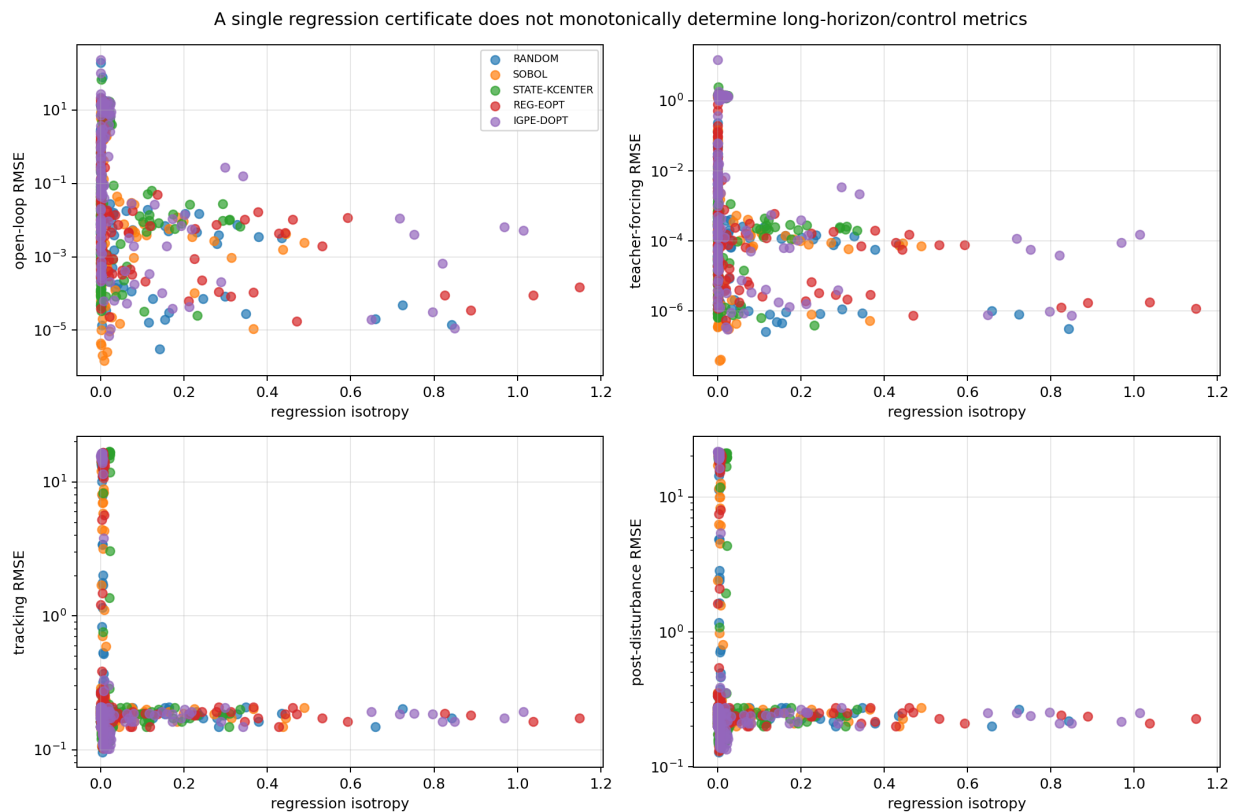


Figure 4: Nonmonotonicity in downstream tasks.

Table 5: IGPE weight sensitivity, reported as mean values. The complete mean [95% CI] table is available at `results/geometry_weight_sensitivity/tables/table9_v4_weight_sensitivity.md`.

system	method	regression_iso	one_step_lift_rmse	open_loop_rmse	tracking_rmse
duffing	IGPE-DOPT	0.0698	0.0523	0.00134	0.181
duffing	IGPE-WHALF	0.0812	0.0375	0.0481	0.181
duffing	IGPE-UNIFORM	0.113	0.0371	0.171	0.181
duffing	IGPE-REG-HEAVY	0.149	0.0474	0.000791	0.181
duffing	IGPE-CLUSTER-HEAVY	0.135	0.0334	0.0302	0.181
lorenz	IGPE-DOPT	0.00944	0.0216	9.72	0.119
lorenz	IGPE-WHALF	0.0142	0.0254	6.83	3.03
lorenz	IGPE-UNIFORM	0.00895	0.0217	11.8	2.02
lorenz	IGPE-REG-HEAVY	0.00849	0.0211	10.1	0.132
lorenz	IGPE-CLUSTER-HEAVY	0.0121	0.0237	11.8	4.12
vdp	IGPE-DOPT	0.0844	0.0387	0.194	0.181
vdp	IGPE-WHALF	0.0551	0.0330	9.10	0.179
vdp	IGPE-UNIFORM	0.167	0.0302	0.465	0.182
vdp	IGPE-REG-HEAVY	0.0522	0.0404	0.116	0.181
vdp	IGPE-CLUSTER-HEAVY	0.0665	0.0413	1.28	0.182

Appendix sanity check: C_{reg} and σ_{min} identity

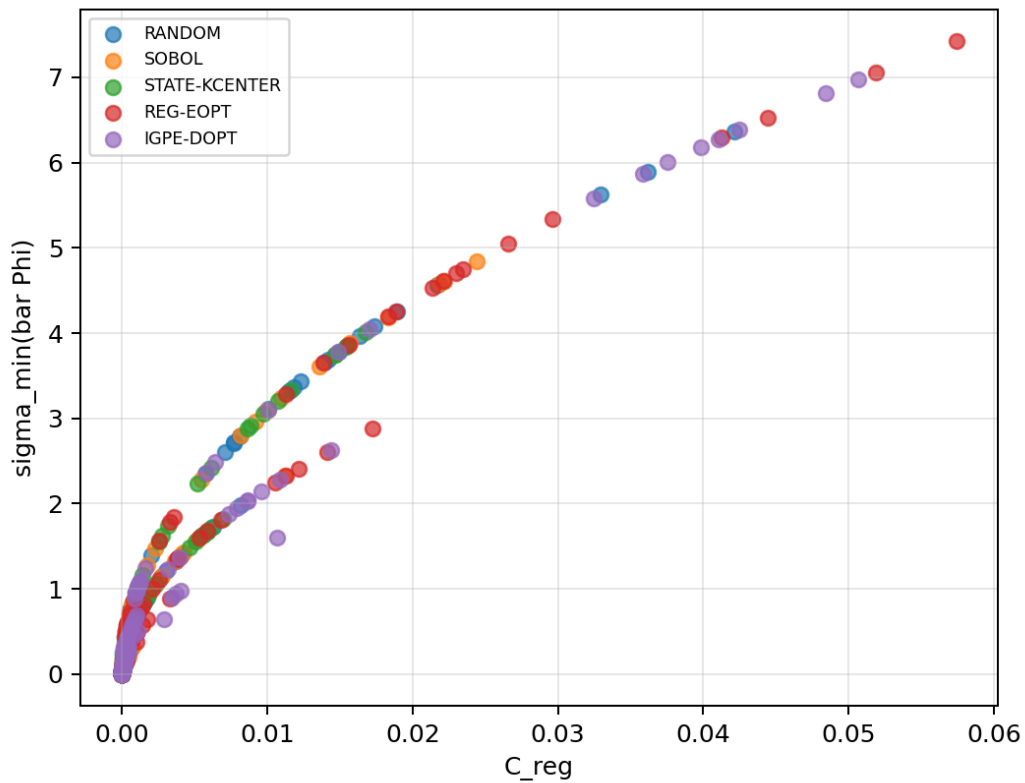


Figure 5: Sanity check for the definitional identity between C_{reg} and the minimum singular value.

Table 6: Lightweight computational-cost benchmark. Times are seconds per single-system case, reported as mean and range over three systems.

method	mean wall-clock	range
RANDOM	0.151	0.145–0.155
SOBOL	0.150	0.147–0.156
STATE-KCENTER	0.163	0.162–0.164
LIFT-DOPT	0.555	0.552–0.561
REG-DOPT	0.561	0.558–0.567
REG-EOPT	0.563	0.553–0.579
A-PE	0.174	0.145–0.206
OID	0.149	0.143–0.153
GPE-STATE	0.168	0.162–0.172
IGPE-DOPT	0.468	0.457–0.476

estimation stability, not long-horizon prediction, closed-loop control, or Koopman invariant-subspace recovery. Fourth, all spectral certificates depend on a fixed dictionary and active-column rules; therefore, reports must jointly provide `active_dim`, `active_rank`, and spectral quantities.

These boundaries are not incidental caveats; they are part of the argument. Table 4 and Figure 4 show that downstream task metrics are not monotone in a single regression certificate. Table 5 shows that weight changes alter the certificate profile, but do not produce a single task-optimal setting. The role of the certificates is to localize data-quality bottlenecks, not to replace task-level validation.

Practitioner guide. In the low-dimensional experiments of this paper, the certificates are most useful as a triage workflow. If active rank is deficient, the first issue is structural: the chosen dictionary, sampling region, or input protocol has produced inactive or redundant regression columns, and adding a small amount of regularization should not be reported as if the design were informative. If active rank is full but `regression_iso` or C_{reg} is small relative to other methods under the same system, dictionary, and budget, the bottleneck is the final EDMDC regression spectrum and a regression-space design such as `REG-EOPT` or the regression term in `IGPE-DOPT` is the natural repair. If state certificates are poor while lifted/regression spectra are also poor, state-space sampling should be repaired first through coverage-oriented strategies such as `STATE-KCENTER`, `GPE-STATE`, or the state terms in `IGPE-DOPT`. If state coverage is high but lifted or regression spectra remain poor, the likely bottleneck is dictionary degeneracy or lack of conditional input excitation relative to lifted features. In all cases, the thresholds are empirical rules for the present low-dimensional settings: compare certificates only after fixing the system, dictionary, standardization rule, budget, and active-column threshold, and then validate the selected design on the downstream prediction or control task.

High-dimensional scalability. The current implementation is intended as a diagnostic prototype, not a high-dimensional optimized solver. Spectral certificates require covariance or Gram-matrix computations whose cost grows with the active lifted dimension. Candidate trajectory scoring multiplies this cost by the number of proposed segments and acquisition rounds. Non-clustering and pairwise coverage diagnostics can become quadratic in the number of samples unless approximate nearest-neighbor, sketching, or minibatch estimators are introduced. Polynomial dictionaries further increase the lifted dimension combinatorially with state dimension and degree, so high-dimensional systems require either structured dictionaries, randomized features, sparse libraries, or incremental spectral updates.

Code and artifact availability. The code, scripts, figures, tables, and LaTeX source used for this revision are prepared as supplementary material in the artifact package accompanying the manuscript. No external repository link is cited in the manuscript; if a public archive is released later, this sentence can be replaced with the archived link and identifier.

Broader impact and ethics. The proposed certificates are diagnostics for data quality and regression identifiability. They are not safety guarantees. In safety-critical control, a favorable certificate profile must still be combined with constraints, robustness analysis, independent validation, failure-mode testing, and human engineering review before deployment.

9 Conclusion

This paper reformulates Koopman/EDMDc data acquisition as a problem of data-quality diagnostics and regression identifiability. Input PE, state coverage, lifted-feature richness, and final EDMDc regression identifiability are different layers and cannot replace one another.

We defined multilayer diagnostic certificates, proved that C_{reg} has direct meaning for one-step EDMDc regression stability, and established a theoretical chain from sampling distributions to empirical regression spectral lower bounds. The state-geometry counterexample and the Schur-complement condition show that the concatenated regression matrix must be inspected directly; reporting only state coverage, lifted-feature rank, or input variance is insufficient.

The experiments show that certificate layers do separate, that budget and weights alter the data-quality profile, and that long-horizon prediction and closed-loop control do not vary monotonically with a single regression certificate. IGPE-DOPT demonstrates the feasibility of certificate-driven sampling, but the contribution of the paper is not a universally optimal sampler. The contribution is a computable, interpretable, ablatable diagnostic framework with explicit theoretical boundaries.

A Reproduction Commands

```
python code/test_improved_gpe.py

python code/improved_gpe_experiments.py major-revision \
  --output-dir results/geometry_major_revision_baselines

python code/improved_gpe_experiments.py major-budget-ablation \
  --output-dir results/geometry_major_revision_budget

python code/improved_gpe_experiments.py degree-ablation \
  --output-dir results/geometry_degree_ablation

python code/improved_gpe_experiments.py component-ablation \
  --output-dir results/geometry_component_ablation

python code/improved_gpe_experiments.py weight-sensitivity \
  --output-dir results/geometry_weight_sensitivity
```

Table 7: Mapping between manuscript objects and code columns.

Manuscript object	Code column
C_{reg}	regression_cov_z_min
$\sigma_{\min}(\bar{\Phi})$	sigma_min_bar_phi
Regression log-det	regression_logdet
Active rank/dimension	active_rank, active_dim
One-step regression error	one_step_lift_rmse, one_step_state_rmse
Composite bottleneck certificate	std_gpe_index

Table 8: Table and figure output files.

Table or figure	File
Table 6 certificate-layer separation	results/geometry_major_revision_budget/tables/table6_v4_certificate_hierarchy.csv, results/geometry_major_revision_budget/tables/table6_v4_certificate_hierarchy.md
Table 7 expanded baseline comparison	results/geometry_major_revision_baselines/tables/table1_summary.csv, results/geometry_major_revision_baselines/tables/table7_v4_external_baselines.md
Table 8 downstream prediction/control metrics	results/geometry_major_revision_budget/tables/table8_v4_downstream_tasks.csv, results/geometry_major_revision_budget/tables/table8_v4_downstream_tasks.md
Table 9 weight sensitivity	results/geometry_weight_sensitivity/tables/table9_v4_weight_sensitivity.csv, results/geometry_weight_sensitivity/tables/table9_v4_weight_sensitivity.md
Figure 6 budget sensitivity	results/geometry_major_revision_budget/figures/figure6_budget_sensitivity.png
Figure 9 certificate-layer separation	results/geometry_major_revision_budget/figures/figure9_certificate_hierarchy.png
Figure 10 regression-theory validation	results/geometry_major_revision_budget/figures/figure10_regression_theory_validation.png
Figure 11 downstream task nonmonotonicity	results/geometry_major_revision_budget/figures/figure11_task_nonmonotonicity.png
Figure A1 sanity check between C_{reg} and minimum singular value	results/geometry_major_revision_budget/figures/figureA1_creg_sigma_min_sanity.png

B Code Metrics and Table/Figure Outputs

References

- Ian Abraham and Todd D Murphey. Active learning of dynamics for data-driven control using koopman operators. *IEEE Transactions on Robotics*, 35(5):1071–1083, 2019. doi: 10.1109/TRO.2019.2923880.
- Nikil Boddupalli, Aqib Hasnain, Sai Pushpak Nandanoori, and Enoch Yeung. Koopman operators for generalized persistence of excitation conditions for nonlinear systems. In *Proceedings of the IEEE 58th Conference on Decision and Control (CDC)*, pages 8106–8111. IEEE, 2019. doi: 10.1109/CDC40024.2019.9029365.
- Steven L Brunton, Marko Budišić, Eurika Kaiser, and J Nathan Kutz. Modern koopman theory for dynamical systems. *SIAM Review*, 64(2):229–340, 2022. doi: 10.1137/21M1401243.
- Salim Dahdah and James Richard Forbes. System norm regularization methods for koopman operator approximation. *Proceedings of the Royal Society A*, 478(2264):20220162, 2022. doi: 10.1098/rspa.2022.0162.

- Arne De Cock, Michel Gevers, and Johan Schoukens. D-optimal input design for nonlinear fir-type systems: A dispersion-based approach. *Automatica*, 73:88–100, 2016. doi: 10.1016/j.automatica.2016.04.052.
- Mario Defflorian and Sebastian Zaglauer. Design of experiments for nonlinear dynamic system identification. In *IFAC Proceedings Volumes*, volume 44, pages 13179–13184. Elsevier, 2011. doi: 10.3182/20110828-6-IT-1002.01502.
- Håkan Hjalmarsson. From experiment design to closed-loop control. *Automatica*, 41(3):393–438, 2005. doi: 10.1016/j.automatica.2004.11.021.
- Mátyás Kiss, Roland Tóth, and Maarten Schoukens. Space-filling input design for nonlinear state-space identification. *IFAC-PapersOnLine*, 58(15):562–567, 2024. doi: 10.1016/j.ifacol.2024.08.589.
- Milan Korda and Igor Mezić. Linear predictors for nonlinear dynamical systems: Koopman operator meets model predictive control. *Automatica*, 93:149–160, 2018. doi: 10.1016/j.automatica.2018.03.046.
- Sahin Lale, Kamyar Azizzadenesheli, Babak Hassibi, and Animashree Anandkumar. Reinforcement learning with fast stabilization in linear dynamical systems. In *Proceedings of the 25th International Conference on Artificial Intelligence and Statistics (AISTATS)*, volume 151 of *Proceedings of Machine Learning Research*, pages 5354–5390. PMLR, 2022. URL <https://proceedings.mlr.press/v151/lale22a.html>.
- Yuqi Liu, Mátyás Kiss, Roland Tóth, and Maarten Schoukens. On space-filling input design for nonlinear dynamic model learning: A gaussian process approach. *IEEE Control Systems Letters*, 9:1868–1873, 2025. doi: 10.1109/LCSYS.2025.3582509.
- Lauren M Miller, Yonatan Silverman, Malcolm A MacIver, and Todd D Murphey. Ergodic exploration of distributed information. *IEEE Transactions on Robotics*, 32(1):36–52, 2016. doi: 10.1109/TRO.2015.2500441.
- Kumpati S Narendra and Anuradha M Annaswamy. Persistent excitation in adaptive systems. *International Journal of Control*, 45(1):127–160, 1987. doi: 10.1080/00207178708933715.
- Anup Parikh, Rushikesh Kamalapurkar, and Warren E Dixon. Integral concurrent learning: Adaptive control with parameter convergence using finite excitation. *International Journal of Adaptive Control and Signal Processing*, 33(12):1775–1787, 2019. doi: 10.1002/acs.2945.
- Friedrich M Philipp, Manuel Schaller, Karl Worthmann, Sebastian Peitz, and Feliks Nüske. Error analysis of kernel edmd for prediction and control in the koopman framework. *Journal of Nonlinear Science*, 35:92, 2025. doi: 10.1007/s00332-025-10182-3.
- Joshua L Proctor, Steven L Brunton, and J Nathan Kutz. Dynamic mode decomposition with control. *SIAM Journal on Applied Dynamical Systems*, 15(1):142–161, 2016. doi: 10.1137/15M1013857.
- Remo Rickenbach, Johannes Köhler, Anna Scampicchio, Melanie N Zeilinger, and Andrea Carron. Active learning-based model predictive coverage control. *IEEE Transactions on Automatic Control*, 69(9):5931–5946, 2024. doi: 10.1109/TAC.2024.3365569.
- Xiaoxue Shang, Jorge Cortés, and Yang Zheng. Willems’ fundamental lemma for nonlinear systems with koopman linear embedding. *IEEE Control Systems Letters*, 2024. doi: 10.1109/LCSYS.2024.3522594.

- V Smits and Oliver Nelles. Space-filling optimized excitation signals for nonlinear system identification of dynamic processes of a diesel engine. *Control Engineering Practice*, 144:105821, 2024. doi: 10.1016/j.conengprac.2023.105821.
- Henk J van Waarde, Jaap Eising, Harry L Trentelman, and M Kanat Camlibel. Data informativity: A new perspective on data-driven analysis and control. *IEEE Transactions on Automatic Control*, 65(11):4753–4768, 2020. doi: 10.1109/TAC.2020.2966717.
- Jan C Willems, Paolo Rapisarda, Ivan Markovsky, and Bart LM De Moor. A note on persistency of excitation. *Systems & Control Letters*, 54(4):325–329, 2005. doi: 10.1016/j.sysconle.2004.09.003.
- Matthew O Williams, Ioannis G Kevrekidis, and Clarence W Rowley. A data-driven approximation of the koopman operator: Extending dynamic mode decomposition. *Journal of Nonlinear Science*, 25:1307–1346, 2015. doi: 10.1007/s00332-015-9258-5.
- Alexander D Wilson, Joshua A Schultz, and Todd D Murphey. Trajectory synthesis for fisher information maximization. *IEEE Transactions on Robotics*, 30(6):1358–1370, 2014. doi: 10.1109/TRO.2014.2345918.